

Spin dynamics, electronic and thermal transport properties of two-dimensional CrPS₄ single crystal

Q. L. Pei¹, X. Luo^{1*}, G.T. Lin¹, J. Y. Song¹, L. Hu¹, Y. M. Zou², L. Yu², W. Tong²,
W. H. Song¹, W. J. Lu¹ and Y. P. Sun^{2,1,3*}

¹ Key Laboratory of Materials Physics, Institute of Solid State Physics, Chinese Academy of Sciences, Hefei, 230031, China

² High Magnetic Field Laboratory, Chinese Academy of Sciences, Hefei, 230031, China

³ Collaborative Innovation Center of Advanced Microstructures, Nanjing University, Nanjing, 210093, China

Abstract

2-Dimensional (2D) CrPS₄ single crystals have been grown by the chemical vapor transport method. The crystallographic, magnetic, electronic and thermal transport properties of the single crystals were investigated by the room-temperature X-ray diffraction, electrical resistivity $\rho(T)$, specific heat $C_p(T)$ and the electronic spin response (ESR) measurements. CrPS₄ crystals crystallize into a monoclinic structure. The electrical resistivity $\rho(T)$ shows a semiconducting behavior with an energy gap $E_g=0.166$ eV. The antiferromagnetic (AFM) transition temperature is about $T_N=36$ K. The spin flipping induced by the applied magnetic field is observed along the c axis. The magnetic phase diagram of CrPS₄ single crystal has been discussed. The extracted magnetic entropy at T_N is about 10.8 J/mol K, which is consistent with the theoretical value $R \ln(2S + 1)$ for $S = 3/2$ of the Cr³⁺ ion. Based on the mean-field theory, the magnetic exchange constants J_l and J_c corresponding to the interactions of the intralayer and between layers are about 0.143 meV and -0.955 meV are obtained based on the fitting of the susceptibility above T_N , which agree with the results obtained from the ESR measurements. With the help of the strain for tuning the magnetic properties, monolayer CrPS₄ may be a promising candidate to explore 2D magnetic semiconductors.

Corresponding author: xluo@issp.ac.cn and ypsun@issp.ac.cn

I Introduction

Two-dimensional (2D) materials have been attracted much attention due to their highly tunable physical properties and immense potential in scalable device applications.[1–4] Especially, the emergence of transition-metal dichalcogenides (TMD) is particularly advantageous as it opens the door to many physical properties not available in graphene.[5–7] For example, in WTe_2 the large magnetoresistance without saturation at the high magnetic field leads to a new direction in the study of magnetoresistivity which might be useful for spintronic applications.[7–8] Another interesting possibility brought by transition-metal elements is the magnetism, which has been investigated to a lesser extent in the current 2D compounds.[9] In this regard, transition-metal tri- or tetra- chalcogenides, such as MnPS_3 and CrPS_4 , represent a rather attractive material family. Similar to dichalcogenides, these compounds also show 2D characteristic with weak interlayer van der Waals interactions. Furthermore, these materials are known to exhibit a large variety of magnetic phases, making them ideal candidates for exfoliated 2D magnets.[10–12]

The layered CrPS_4 crystallizes into a monoclinic symmetry.[13,14] The sulfur layers are hexagonally close-packed, the Cr atoms are localized in the octahedral holes of S atoms and P atoms are surrounded by four S atoms in tetrahedral coordination. The van der Waals gaps exist between the sulfur layers along the c axis and the cleaving surface is parallel to the ab plane. The Cr-based compound CrPS_4 was synthesized thirty years ago, and an antiferromagnetic (AFM) temperature $T_N=36$ K of the insulating CrPS_4 was just reported.[14] To explore the possible exfoliated 2D magnet in CrPS_4 , the motivation of the present paper aims to gain a better understanding of the bulk properties of CrPS_4 single crystal so that future studies on single-layer CrPS_4 will have a firmer foundation. Herein, we did the research by the magnetization, electronic, thermal transport and the electronic spin response (ESR) measurements on the layered CrPS_4 single crystal.

II Experimental results

Single crystalline specimens of CrPS_4 were prepared by the chemical vapor transport method. Cr powders (99.99 %, Alfa Aesar), red P powders (99.99 %, Alfa Aesar) and S powders (99.99 %, Alfa Aesar) with mole ratio 1:1:4 were weighted and loaded into a silicon quartz tube, which was sealed under high vacuum. All were done in an Ar-filled glove box. The sealed quartz tubes were

put in a two-zone tube furnace. The hot side is about 650 °C while the cold side is about 550 °C, and dwelled for 7 days, then slowly cooled down to room temperature with 100°C per hour. Hexagonal shape single crystals with shining surface were observed. The size of the crystal was about 4*6*0.5 mm³. The single crystals were air-stable and soft and can be easily exfoliated. Powder X-ray diffraction (XRD) patterns were taken with Cu $K_{\alpha 1}$ radiation ($\lambda=0.15406$ nm) using a PANalytical X'pert diffractometer at room temperature. The magnetic properties were carried out by the magnetic property measurement system (MPMS-XL5). The electrical transport measurements were performed by a four-probe method to eliminate the contact resistance. The measurement of specific heat was carried out by a heat-pulse relaxation method on Physical Properties Measurement System (PPMS-9T). The ESR measurement of the CrPS₄ single crystal was performed using a Bruker EMX plus model spectrometer operating at X-band frequencies (9.4 GHz) at different temperatures.

III Results and discussion

The CrPS₄ crystallizes into a layered structure. As shown in the inset of Fig. 1 (a), hexagonal-close-packed sulfur layers parallel to the bc plane are the fundamental basis of the crystal structure and the Cr and P atoms are in distorted octahedral and tetrahedral interstices, respectively. The powdered XRD data were collected on crushed single crystals of CrPS₄ at room temperature as shown in Fig. 1 (a). It also presents the structural Rietveld refinement profiles of the XRD data using FullProf software.[15] The refinements of the XRD data indicate that the crystals are single-phase since no extra peaks were observed. The fitted parameters are shown in the Table I. The flat surface was identified as the (001) planes, as shown in the Fig. 1 (b) and the crystal used is presented in the inset of Fig. 1 (b).

In order to investigate the macroscopic magnetic properties of the CrPS₄ single crystal, we carried out the measurement of the magnetization as the function of temperature and magnetic field. Figure 2 shows the temperature dependence of magnetization ($M(T)$) under the zero-field-cooled (ZFC) and field-cooled (FC) modes with the applied magnetic field $H= 0.01$ T. Fig. 2 (a) and (b) show the $M(T)$ with H parallel and perpendicular to the c axis, respectively. The Néel temperature T_N is observed around 36 K, which is consistent with the reported data.[14] The magnetization below the T_N is anisotropic with $M_{ab} > M_c$, which indicates that the easy

magnetization axis is along the direction of the c axis.[16] In the paramagnetic (PM) state, the temperature dependence of susceptibility ($\chi(T)$) follows the Curie-Weiss law shown by solid lines in insets of Fig.2 (a) and (b). The Curie-Weiss law for the magnetic susceptibility χ is described as follows:

$$\chi(T) = \frac{M}{H} = \frac{C}{T-\theta_P} + \chi_0 \quad (1)$$

Where C is the Curie constant, θ_P is the Weiss temperature and χ_0 is the Pauli PM constant. From the least-square analysis by Eq. (1), we can obtain the Weiss temperature $\theta_P(H//c) = \theta_P(H \perp c) = 19.4$ K and Curie constant $C(H//c) = 4.23$ emu K/mol, $C(H \perp c) = 4.13$ emu K/mol, respectively.

The effective magnetic moment μ_{eff} can be obtained by:

$$\mu_{eff}/\mu_B = \sqrt{3k_B C/N_A Z} \quad (2a)$$

where $k_B = 1.38 \times 10^{-16}$ erg/K, $N_A = 6.02 \times 10^{23}$ mol⁻¹ and Z is the atom number per unit cell. The value of μ_{eff} can be simplified:

$$\mu_{eff} = \sqrt{8C}\mu_B \quad (2b)$$

From the Eq. (2b), we can get the effective magnetic moment μ_{eff}

$$\mu_{eff} = \sqrt{8C}\mu_B = 5.8\mu_B \quad (H//c) \quad (2c)$$

$$\mu_{eff} = \sqrt{8C}\mu_B = 5.74\mu_B \quad (H \perp c) \quad (2d)$$

The theoretical value of Cr³⁺ ion can be estimated by:

$$\mu_{eff} = g\sqrt{S(S+1)}\mu_B = 3.87\mu_B \quad (3)$$

where the value of g is 2. The experimental values of μ_{eff} are larger than the theoretical value of Cr³⁺ ion, which may be related to the strong spin-lattice coupling existing above the T_N in 2D CrPS₄ single crystal.[1]

In order to further investigate the nature of the AFM structure of CrPS₄ single crystal, the magnetic field dependence of the magnetization ($M(H)$) for CrPS₄ single crystal with different directions at $T=5$ K are shown in Fig. 3 (a) and (b), respectively. Interestingly, a magnetic switching effect is observed when the magnetic field is along the c axis, as shown in Fig. 3 (a). The critical field H_C is about 0.9 T at $T=5$ K. As the measuring temperature is varied, it is found that the critical field H_C changes as shown in the main panel of Fig. 3(c). The evolution of the critical field H_C with the different measuring temperatures is shown in of Fig. 3 (d), indicating the monotonous reduction of H_C with increasing measuring temperatures. The magnetic switching

effect disappears when the measuring temperature is close to the T_N . We try to further understand the possible magnetic ground state of CrPS₄ single crystal and compare the $M(H)$ at $T=5$ K and $H>H_C$ along different directions. As shown in Fig. 3 (a) and (b), above H_C , the values of $M(H)$ along different directions are nearly the same, which may be due to the similar magnetic structure for the different directions. The similar character is also reported in EuCu₂As₂ and EuCu₂Sb₂, [16] the possible magnetic structure of CrPS₄ is presumed in Fig. 4 (a) and (b). Below H_C , as shown in Fig. 4 (a), the Cr³⁺ moments are antiferromagnetically aligned in the ab plane and ferromagnetically aligned along the c axis, that is the collinear C-type AFM structure. The $M(T)$ in Fig. 2 also consists with a collinear C-type AFM structure, where the easy magnetization axis is along the direction of c axis. When $H>H_C$, the magnetic structure is supposed to change into G-type AFM structure, as shown in Fig. 4(b). The Cr³⁺ moments are antiferromagnetically aligned both in the ab plane and along the c axis. The G-type AFM structure is the stable magnetic state under the applied magnetic field. Fig. 4 (c) presents the possible magnetic phase diagram of CrPS₄ single crystal.

Based the Molecular Field Theory (MFT), we can estimate the exchange interactions. [18] In MFT, the value f_j arising from the exchange interactions as:

$$f_j = \frac{\theta_{pJ}}{T_{NJ}} = 0.54 \quad (H // c) \quad (4)$$

θ_{pJ} and f_j are related to the exchange interactions by the following functions:

$$T_{NJ} = -\frac{S(S+1)}{3k_B} \sum_j J_{ij} \cos \phi_{ji} \quad (5a)$$

$$\theta_{pJ} = -\frac{S(S+1)}{3k_B} \sum_j J_{ij} \quad (5b)$$

$$f_j = \frac{\sum_j J_{ij}}{\sum_j J_{ij} \cos \phi_{ji}} \quad (5c)$$

i means the center spin and j means all neighbors, while J_{ij} is the respective exchange constant and ϕ_{ij} is the angle between ordered moments μ_j and μ_i in the magnetic order state. The sums are around all neighbors j with which a central spin i interacts.

Based on the C-type AFM, we can calculate the exchange interactions of the CrPS₄ single crystal, which has fourfold in-plane nearest neighbor interaction J_1 (J_a and J_b are the magnetic interactions along the a and b axis in ab plane, based on the C-type AFM structure, J_a and J_b are AFM interaction. Because we cannot distinguish the interactions along a and b axes, J_1 is the

average value of J_a and J_b .) and twofold interlayer interaction J_c , we can obtain:

$$T_{NJ} = -\frac{S(S+1)}{3k_B}(2J_c - 4J_1) \quad (6a)$$

$$\theta_{pJ} = -\frac{S(S+1)}{3k_B}(2J_c + 4J_1) \quad (6b)$$

$$f_J = \frac{\theta_{pJ}}{T_{NJ}} = \frac{2J_1 + J_c}{2J_1 - J_c} \quad (6c)$$

We obtain $J_1 = 0.143 \text{ meV}$, $J_c = -0.955 \text{ meV}$. J_1 is AFM interaction with positive value and J_c is FM one with negative one, which are consistent with the C-type AFM structure. However, the further experiments, such as neutron scattering experiment, are really needed to determine the magnetic structure of CrPS₄ single crystal.

As to the transport properties of CrPS₄ single crystal, Figure 5 shows the temperature dependence of the resistivity in the ab plane for CrPS₄ single crystal. The $d\rho/dT$ is negative and CrPS₄ single crystal shows a semiconducting behavior. In the inset of Fig.5, $\ln(\rho)$ decreases almost linearly with increasing T from 175 K to 300 K, we can calculate the activation energy by using Arrhenius equation:[18]

$$\ln \rho = \ln \rho_0 - \frac{E_a}{k_B T} \quad (7)$$

As shown in the inset of Fig.5, the activation energy E_a is about 0.166 eV.

To study the thermal property, we perform the measurement of specific heat of CrPS₄ single crystal. Fig.6 (a) shows the temperature dependence of the heat capacity C_P for CrPS₄ single crystal. The $C_P(T)$ of CrPS₄ exhibits a anomaly around $T_N = 36 \text{ K}$. Because of the thin flake crystal with small mass, a sharp λ -type peak has not been observed around $T_N=36 \text{ K}$. Since CrPS₄ shows insulating behavior, we can ignore the electronic contribution to the heat capacity, the $C_{mag}(T)$ can be calculated by the following equations:[18]

$$C_{V \text{ Debye}}(T) = 9R \left(\frac{T}{\theta_D}\right)^3 \int_0^{\theta_D/T} \frac{x^4 e^x}{(e^x - 1)^2} dx \quad (8a)$$

$$C_{mag}(T) = C_P(T) - nC_{V \text{ Debye}}(T) \quad (8b)$$

while $n = 6$ is the number of atoms per formula unit, R is the molar gas constant and θ_D is the Debye temperature. As shown in Fig. 6 (b), the solid line is the calculated lattice contribution of the heat capacity. The fitted Debye temperature θ_D is about 502 K. We can get the $C_{mag}(T)$ based on the MFT [18], the heat-capacity jump at the magnetic transition can be calculated for the two possible magnetic structures: (1) the equal moment (EM) structure where the magnetic moments

are the same at all sites and (2) the amplitude modulated (AM) structure where the magnetic-moment amplitude varies periodically from one site to another one. For EM structure, the jump in the heat capacity at the ordering temperature is given by [19]

$$\Delta C_{EM} = 5 \frac{J(J+1)}{(2J^2+2J+1)} R \quad (9a)$$

and for AM structure,

$$\Delta C_{AM} = \frac{10}{3} \frac{J(J+1)}{(2J^2+2J+1)} R \quad (9b)$$

where J is the total angular momentum and R is the gas constant. By using $J=3/2$ for Cr^{3+} , ΔC_{EM} and ΔC_{AM} are calculated to 18.2 J/mol K and 12.2 J/mol K, respectively. Our estimated $\Delta C_{mag} \approx 10.8$ J/mol K is close to the value of ΔC_{AM} , which indicates that CrPS_4 possesses an AM structure. The AM structure obtained from the heat capacity measurement is consistent with the above discussed C-type AFM magnetic structure. The magnetic contribution to the entropy S_{mag} was obtained by integrating the C_{mag}/T versus T : [18]

$$S_{mag}(T) = \int_0^T \frac{C_{mag}(T)}{T} dT \quad (10)$$

The T dependence of S_{mag} is shown in Fig. 6 (c) for the temperature range from 5 K to 100 K. The theoretical expected value of the magnetic contribution to the entropy is $S_{mag}(T) = R \ln(2S+1) = R \ln 4 = 11.5$ J/mol K (for Cr^{3+} , $S = 3/2$), which is shown by the dashed curve in Fig.6 (c). Fig.6 (c) indicates that the value of S_{mag} is about 85 % of the theoretical expected value.

In order to investigate further the magnetic property of CrPS_4 single crystal, we perform its ESR spectra measurement. Fig. 7 (a) and (b) shows the ESR spectra of CrPS_4 single crystal at selected temperatures under the applied field from 0 to 0.6 T, which is applied along the different crystallographic axes. The signal consists of a single exchange-narrowed resonance line, which can be well fitted by a Lorentz shape at resonance field H_r with the linewidth ΔH and the half width at half maximum as shown in Fig.8 (a) and (b). The function of Lorentz line is [20]:

$$Y' = -Y_{max} \frac{2\Delta H^2(H-H_r)}{[\Delta H^2+(H-H_r)^2]^2} \quad (11a)$$

$$Y = Y_{max} \frac{\Delta H^2}{\Delta H^2+(H-H_r)^2} \quad (11b)$$

$$Y_{max} = Y|_{H=H_r} \quad (11c)$$

The temperature dependence of the effective g values along different directions are plotted in Fig. 8 (c) and (d). The g values at different temperatures are obtained from resonance field H_r and the

microwave frequency ν via the Larmor condition [20]:

$$h\nu = g\mu_B H_r \quad (12)$$

The calculated g values are around 1.98, which is in good agreement with the previously reported result of $g_{Cr^{3+}} = 1.978$ [21].

Figure 8 (e) and (f) display the normalized ESR intensity I by its value at 300 K as a function of temperature. We obtain the value of I according to the following function:

$$I = \int_{+\infty}^0 Y dH \quad (13)$$

which can be described by a thermally activated model, and well fitted by the Arrhenius law [22]:

$$I \propto \exp(\Delta E/k_B T) \quad (14)$$

where ΔE is the activation energy. The insets of Fig.8 (e) and (f) show $\ln I/I(T=300 \text{ K})$ vs. $1000/T$. According to Eq. (14), we can obtain the activation energy $\Delta E(H//c)=0.0135 \text{ eV}$ and $\Delta E(H \perp c)=0.0144 \text{ eV}$.

The angular dependence of the ESR linewidth includes the more information on the exchange interaction. As shown in Fig. (9), we investigate the angular dependence of the ESR linewidth in detail for three crystallographic planes at $T=150 \text{ K}$. The three lines are corresponding to a set of orthogonal axes: the black line is corresponding to the applied field H perpendicular to the c axis and red lines are corresponding to a pair of orthogonal axes lying in the ab plane.

The ESR linewidth ΔH can be fitted via the relation between the second moment M_2 [23, 24]:

$$\Delta H = \frac{\hbar}{g\mu_B \omega_{ex}} M_2 \quad (15)$$

where ω_{ex} is so-called exchange frequency. In this article, we use the experimental value of $g = 1.98$, which is obtained from the ESR measurement.

The second moment M_2 is given by:

$$M_2 = 2 \frac{S(S+1)}{3} \left\{ f_1 (2\tilde{J}_{zz} - \tilde{J}_{xx} - \tilde{J}_{yy})^2 + f_2 \times 10(\tilde{J}_{xz}^2 + \tilde{J}_{yz}^2) + f_3 \left[(\tilde{J}_{xx} - \tilde{J}_{yy})^2 + 4\tilde{J}_{xy}^2 \right] \right\} \quad (16)$$

The symbols f_1, f_2 and f_3 denote the spectral-density functions. [23, 24]

The angular dependence of the ESR linewidth at $T=150 \text{ K}$ can be well fitted. The fitting solid lines are illustrated in Fig. (9). The obtained parameters are following: $J_1/J_c = -0.635$ with $J_1 > 0$ and $J_c < 0$. $J_1 > 0$ means AFM interaction in ab plane and $J_c < 0$ means FM interaction interlayer, which are again in agreement with the C-type AFM structure discussed above. However, the value of J_1/J_c is smaller than the value obtained from the magnetization result mentioned above. The

framework of our model is simple and does not include other interactions. For example, Dzyaloshinsky-Moriya (DM) interaction may result in the tilting of the CrS_6 octahedra along the antiferromagnetically coupled along c axis, which can induce line broadening of comparable order of magnitude.[25]

As it is well known, many chalcogenides form layered structures and can be exfoliated, the complexity of bulk crystals can be well tuned in the single- and few-layer materials. Recently, monolayer of the Cr-based tri-chalcogenides, such as $\text{Cr}(\text{Si}, \text{Ge} \text{ and } \text{Sn})\text{Te}_3$, have been well studied by the first principle calculations, which show that the physical properties of monolayer Cr-based tri- chalcogenides is very sensitive to the strain effecting.[15, 26, 27] For example, for CrSiTe_3 , with the help of the strain, the ground state can be well tuned from AFM semiconductor to FM one. The FM Curie temperature of the monolayer CrSiTe_3 can be up to 156 K. Herein, we compare the exchange interactions between the 2D AMX_3 compounds and CrPS_4 , as shown in **Table IV**.[28] The bulk CrPS_4 single crystal shows a similar character with the 2D AMX_3 materials. That means with the application of a moderate uniform in-plane tensile strain of 3-4 %, which is experimentally feasible, the ground state may be tunable from AFM semiconductor of bulk CrPS_4 into FM one in monolayer CrPS_4 . On the other hand, compared with $\text{Cr}(\text{Si}, \text{Ge} \text{ and } \text{Sn})\text{Te}_3$, there are some advantages for CrPS_4 single crystal. One is that the monolayer of CrPS_4 can be easily obtained by exfoliating because CrPS_4 single crystal is soft. Another advantage is that the CrPS_4 single crystal is very stable in air, which is good for fabricating the heterojunction with other chalcogenides in the spintronic application. Therefore, the monolayer CrPS_4 may be a promising candidate to explore 2D magnetic semiconductors. However, it is still an open question, further research, such as the first-principle calculations or the investigation on the mono-layer CrPS_4 crystal or CrPS_4 film are really needed.

IV Conclusion

The detailed physical properties of the layered compound CrPS_4 single crystal were investigated by the room-temperature X-ray diffraction, electrical resistivity $\rho(T)$, and specific heat $C_p(T)$. CrPS_4 crystals crystallize into a monoclinic structure. The electrical resistivity $\rho(T)$ shows an insulator behavior with an energy gap $E_g=0.167$ eV. The AFM transition temperature is about $T_N=36$ K. The exchange constants J_l and J_c corresponding to the intralayer and interlayer

interaction are about 0.143 meV and -0.955 meV . The magneto-switching effect is obtained along the c axis, which may be related to the change of magnetic structure induced by the applied magnetic field. The possible magnetic phase diagram of CrPS_4 single crystal has been presented. The extracted magnetic entropy at T_N is consistent with the theoretical value $R \ln(2S + 1)$ for $S = 3/2$ of the Cr^{3+} ion. It is suggested that monolayer CrPS_4 may be a promising candidate to explore 2D magnetic semiconductors with the help of the strain effect.

Acknowledgement

This work was supported by the Joint Funds of the National Natural Science Foundation of China and the Chinese Academy of Sciences' Large-Scale Scientific Facility under contracts (U1432139, U1232139), the National Nature Science Foundation of China under contracts (51171177, 11404342), the National Key Basic Research under contract 2011CBA00111, and the Nature Science Foundation of Anhui Province under contract 1508085ME103, 1408085MA11.

References:

- [1] K. S. Novoselov, A. K. Geim, S. V. Morozov, D. Jiang, Y. Zhang, S. V. Dubonos, I. V. Grigorieva, and A. A. Firsov. Electric field effect in atomically thin carbon films, *Science* **2004**, 306, 666-669.
- [2] K. S. Novoselov, A. K. Geim, S. V. Morozov, D. Jiang, M. I. Katsnelson, I. V. Grigorieva, S. V. Dubonos, and A. A. Firsov. Two-dimensional gas of massless diracfermions in graphene, *Nature* **2005**, 438, 197-200.
- [3] Y. Zhang, Y. -W. Tan, H. L. Stormer, and P. Kim. Experimental Observation of Quantum Hall Effect and Berry's Phase in Graphene, *Nature* **2005**, 438, 201-204.
- [4] A. H. Castro Neto, F. Guinea, N. M. R. Peres, K. S. Novoselov, and A. K. Geim. The electro properties of graphene, *Rev. Mod. Phys.* **2009**, 81, 109-162.
- [5] Y. J. Yu, F. Y. Yang, X. F. Lu, Y. J. Yan, Y. H. Cho, L.G. Ma, X. H. Niu, S. Kim, Y.-W. Son, D. L. Feng, S. Y. Li, S.-W. Cheong, X. H. Chen, and Y. B. Zhang. Gate-tunable phase transitions in thin flakes of 1T-TaS₂, *Nature Nanotechnology* **2015**, 10, 270-276.
- [6] L. K. Li, Y. J. Yu, G. J. Ye, Q. Q. Ge, X. D. Du, H. Wu, D. L. Feng, X. H. Chen, and Y. B. Zhang. Black Phosphorus Field-effect Transistors, *Nature Nanotechnology* **2014**, 9, 372-377.
- [7] M. N. Ali, J. Xiong, S. Flynn, J. Tao, Q. D. Gibson, L. M. Schoop, T. Liang, N. Haldolaarachchige, M. Hirschberger, N. P. Ong, and R. J. Cava. Large, non-saturating magnetoresistance in WTe₂, *Nature* **2014**, 514, 205-208.
- [8] L. R. Thoutam, Y. L. Wang, Z. L. Xiao, S. Das, A. Luican-Mayer, R. Divan, G. W. Crabtree, and W. K. Kwok. Temperature dependent three-dimensional anisotropy of the magnetoresistance in WTe₂, *Phys. Rev. Lett.* **2015**, 115, 046602.

- [9] M. A. McGuire, H. Dixit, V. R. Cooper, and B. C. Sales. ChemInform Abstract: Coupling of Crystal Structure and Magnetism in the Layered, Ferromagnetic Insulator CrI₃, *Chem. Mater.* **2015**, *27*, 612-620.
- [10] R. Brec. Review on structural and chemical properties of transition metal phosphorous trisulfides MPS₃, *Solid State Ionics* **1986**, *22*, 3-30.
- [11] T. Masubuchi, H. Hoya, T. Watanabe, Y. Takahashi, S. Ban, N. Ohkubo, K. Takase, and Y. Takano. Phase diagram, magnetic properties and specific heat of Mn_{1-x}Fe_xPS₃, *J. Alloys and Compounds* **2008**, *460*, 668-674.
- [12] A. R. Wildes, B. Roessli, B. Lebech, and K. W. Godfrey. Spin waves and the critical behaviour of the magnetization in MnPS₃, *J. Phys.: Condens. Matter* **1998**, *10*, 6417-6428.
- [13] R. Diehl and D. Carpentier. The Crystal Structure Of Chromium Thiophosphate, CrPS₄, *Acta Crystl. B* **1977**, *33*, 1399-1404.
- [14] A. Louisy, G. Ouvrard, D. M. Schleich, and R. Brec. Physical properties and lithium intercalates of CrPS₄, *Solid State Communications* **1978**, *28*, 61-66.
- [15] J. Rodríguez-Carvajal. Recent advances in magnetic structure determination by neutron powder diffraction, *Physica B* **1993**, *192*, 55-69; see also www.ill.eu/sites/fullprof/
- [16] V. K. Anand, and D. C. Johnston, *Phy. Rev. B* **2015**, *91*, 184403.
- [17] L. D. Casto, A. J. Clune, M. O. Yokosuk, J. L. Musfeldt, T. J. Williams, H. L. Zhuang, M. -W. Lin, K. Xiao, R. G. Hennig, B. C. Sales, J. -Q. Yan, and D. Mandrus, *APL Materials*, **2015**, *3*, 041515.
- [18] C. Kittel, *Introduction to Solid State Physics*, 4th ed.; Wiley: New York, **1966**.
- [19] J. A. Blanco, D. Gignoux, and D. Schmitt. Specific heat in some gadolinium compounds. II.

- Theoretical model, *Phys. Rev. B* **1991**, 43, 13145-13151.
- [20] J. A. Weil and J. R. Bolton, *Electron Paramagnetic Resonance. Elementary Theory and Practical Applications*, John Wiley, U.S.A., **1994**.
- [21] M. A. Fayzullin, R. M. Eremina, M. V. Eremin, A. Dittl, N. van Well, F. Ritter, W. Assmus, J. Deisenhofer, H.-A. Krug von Nidda, and A. Loidl. Spin correlations and Dzyaloshinskii-Moriya interaction in Cs_2CuCl_4 , *Phys. Rev. B* **2013**, 88, 174421.
- [22] E. Winkler, S. Blanco Canosa, F. Rivadulla, M. A. López-Quintela, J. Rivas, A. Caneiro, M. T. Causa, and M. Tovar. Magnetocrystalline interactions in MnCr_2O_4 spinel, *Phys. Rev. B* **2009**, 80, 104418.
- [23] J. Deisenhofer, M. V. Eremin, D. V. Zakharov, V. A. Ivanshin, R. M. Eremina, H.-A. Krug von Nidda, A. A. Mukhin, A. M. Balbashov, and A. Loidl. Crystal field, Dzyaloshinsky-Moriya interaction, and orbital order in $\text{La}_{0.95}\text{Sr}_{0.05}\text{MnO}_3$ probed by ESR, *Phys. Rev. B* **2002**, 65, 104440.
- [24] R. Kubo and K. Tomita. A General Theory of Magnetic Resonance Absorption, *J. Phys. Soc. Jpn.* **1954**, 9, 888-919.
- [25] H. -A. Krug von Nidda, L. E. Svistov, M. V. Eremin, R. M. Eremina, A. Loidl, V. Kataev, A. Validov, A. Prokofiev, and W. Assmus. Anisotropic exchange in LiCuVO_4 probed by ESR, *Phys. Rev. B* **2002**, 65, 134445.
- [26] N. Sivadas, M. W. Daniels, R. H. Swendsen, S. Okamoto and D. Xiao. Magnetic ground state of semiconducting transition metal trichalcogenide monolayers, *Phys. Rev. B* **2015**, 91, 235425.
- [27] Houlong L. Zhuang, Yu Xie, P. R. C. Kent, and P. Ganesh. Computational discovery of ferromagnetic semiconducting single-layer CrSnTe_3 , *Phys. Rev. B* **2015**, 92, 035407.
- [28] A. Gupta, T. Sakhivel, and S. Seal, *Progress in Materials Science*, **2015**, 73, 44-126.

Table I: Crystallographic parameters of CrPS₄ single crystal.

Atom	Wyckoff position	<i>x</i>	<i>y</i>	<i>z</i>
Cr	<i>4g</i>	0	0.2481	0
P	<i>4i</i>	0.2971	0	0.1655
S1	<i>8j</i>	0.1341	0.2666	0.7
S2	<i>4i</i>	0.1062	0	0.1934
S3	<i>4i</i>	0.1303	0.5	0.1452

Table II: Crystallographic and Rietveld refinement obtained from powder XRD data.

Crystal system	hexagonal
Space group	<i>C</i> _{12/m1} (No.12)
Wavelength	1.5406 (<i>Cu Kα</i>)
Unit cell	
<i>a</i> (Å)	10.871
<i>b</i> (Å)	7.254
<i>c</i> (Å)	6.14
β (°)	91.88
<i>V</i> (Å ³)	483.929
<i>Z</i>	4
<i>d</i> _{Cr-S} (Å)	2.39
	2.4275
	2.4611
<i>d</i> _{P-S} (Å)	2.0168
	2.0879
	2.0883
ρ_{calc} (g/cm ³)	2.9
χ^2	2.866
<i>R</i> _p	9.414
<i>R</i> _{wp}	8.211

Table III: The physical parameters for CrPS₄ single crystal.

parameters	CrPS ₄
T_N (K)	36
μ_{eff}	6.47 μ_0 ($H // c$)
	6.41 μ_0 ($H \perp c$)
Θ (K)	19.4
J_1 (meV)	0.143
J_C (meV)	-0.955
$\rho(300\text{ K})$ ($\Omega\text{ cm}$)	1.2×10^3
E_a (eV)	0.166
Θ_D (K)	502
ΔC_{mag} (J/mol K)	10.8
S_{mag} (J/mol K)	11.5
ΔE (eV)	0.0135 ($H // c$)
	0.0144 ($H \perp c$)

Table IV: Lattice constant a , magnetic ground state and magnetic critical temperature for reported ABX₃ and CrPS₄.

	a (\AA)	Ground state	J (meV)	T_C (T_N) (K)	Ref.
MnPSe ₃	6.27	AFM-Néel	0.46	147	28
MnPSe ₃ (2 % strain)	6.40	AFM- Néel	0.33	115	28
CrSiTe ₃	6.84	AFM-zigzag	-0.74	160	28
CrSiTe ₃ (4% strain)	7.11	FM	-2.29	158	28
CrPS ₄	10.871	C-type AFM	0.143	36	this work

Figure 1:

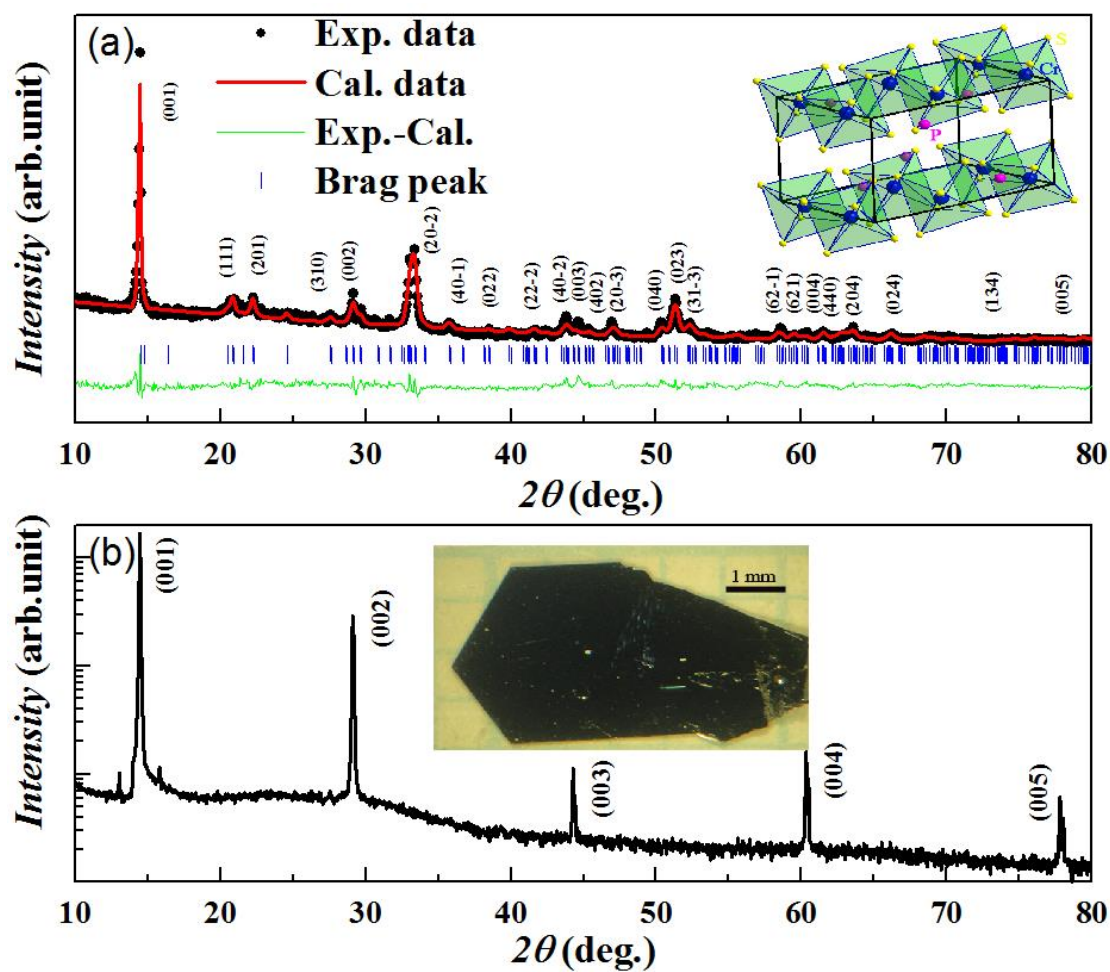


Fig. 1(color online): (a) The Rietveld refined powder XRD patterns at room temperature for the crushed CrPS₄ crystals. The vertical marks (blue bars) stand for the position of Bragg peaks, and solid line (green line) at the bottom correspond to the difference between experimental and calculated intensities. Inset shows the crystal structure of CrPS₄ drawn based on the XRD refinement. (b) XRD patterns of the crystal measured on the (001) surface. Inset presents the picture of the CrPS₄ single crystal used for this study. The crystal size is approximately 4*6*0.5 mm.

Figure 2:

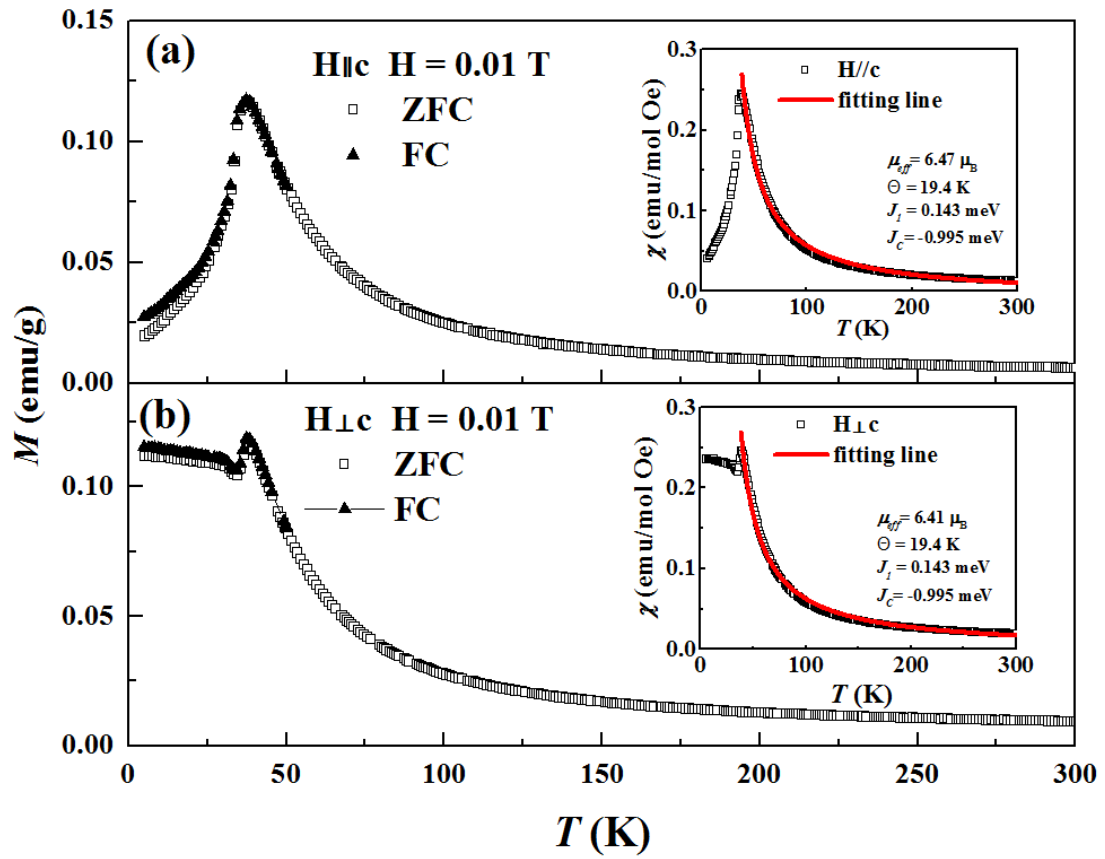


Fig. 2 (color online): The temperature dependence of magnetization of CrPS₄ single crystal under ZFC and FC models with applied magnetic field $H=0.01$ T. (a) for applied magnetic field parallel to the c axis and (b) for the applied magnetic field perpendicular to the c axis. The insets of (a) and (b) show the fitting results according to the Eq. (1).

Figure 3:

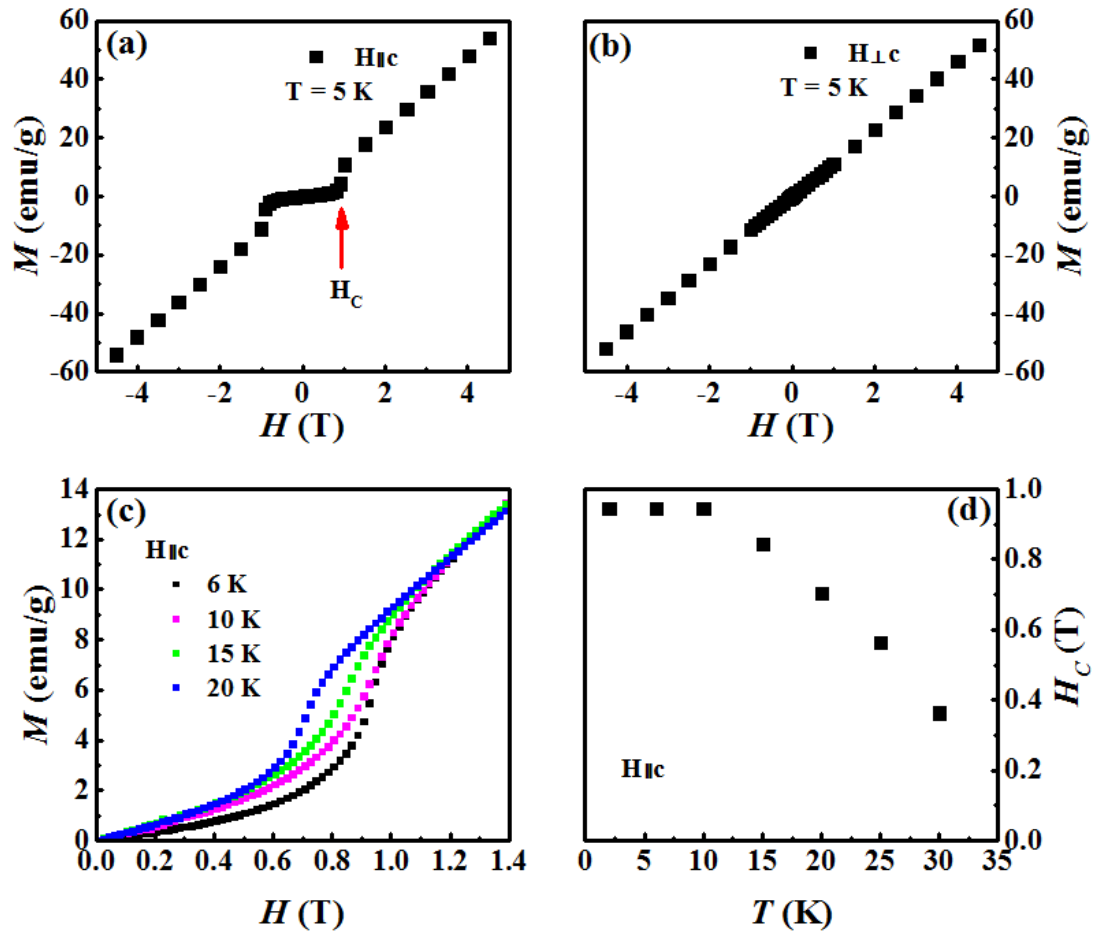


Fig. 3 (color online): (a) and (b) show the magnetic field dependence of magnetization at $T=5$ K for H parallel and perpendicular to the c axis, respectively. (c) shows the magnetic field dependence of magnetization at different temperatures. (d) presents the temperature dependence of critical field (H_c).

Figure 4:

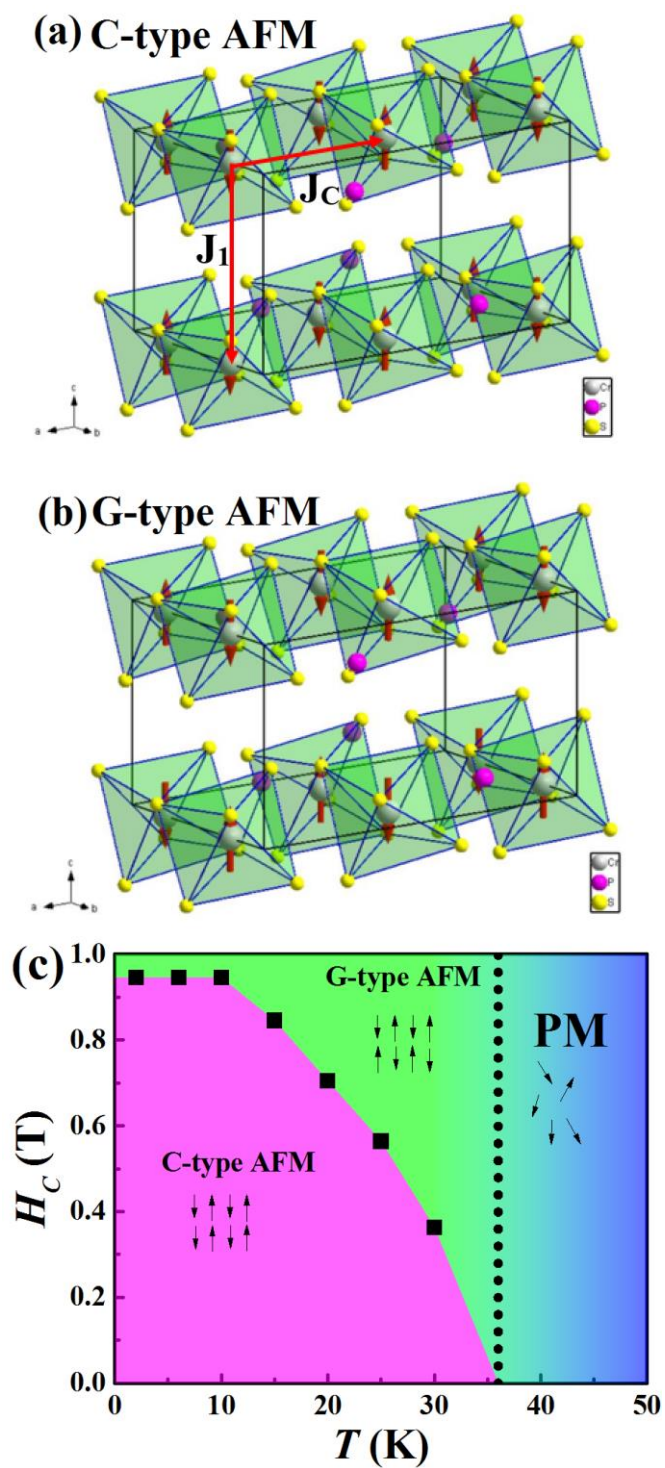


Fig. 4 (color online): The magnetic structures of CrPS₄ (a) the C-type AFM below the critical magnetization H_c ; (b) G-type AFM for the magnetic structure above the H_c and (c) The magnetic phase diagram of CrPS₄.

Figure 5:

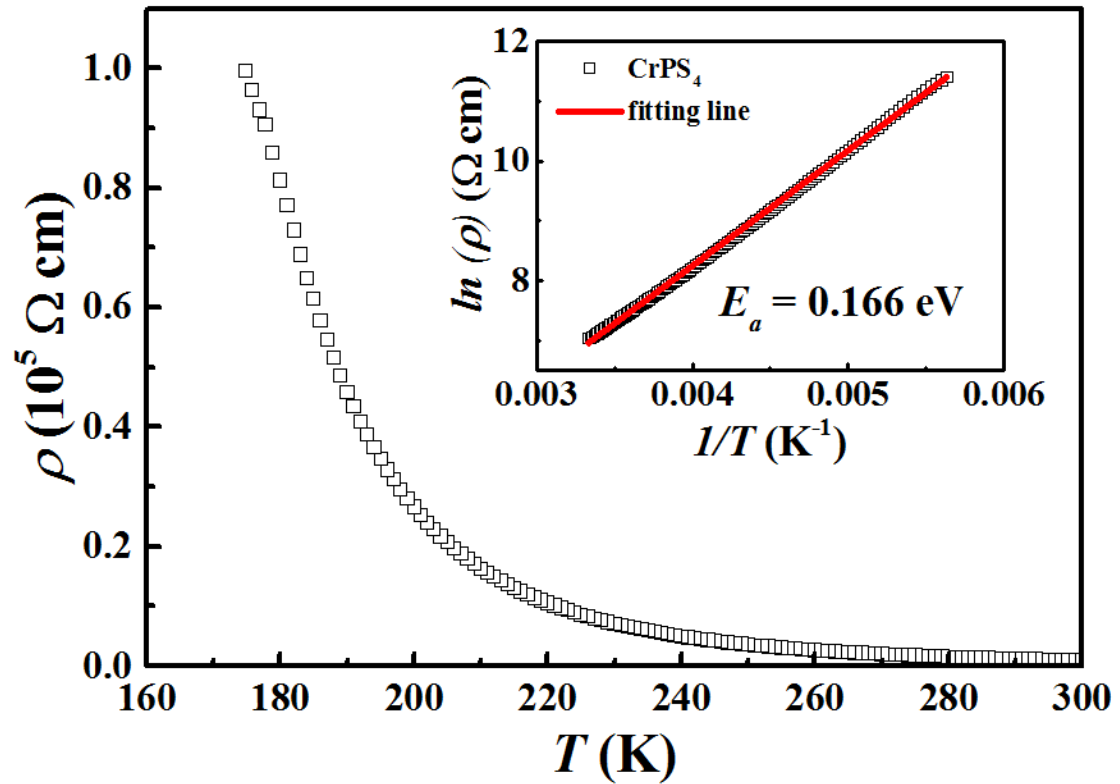


Fig. 5 (color online): The temperature dependence of resistivity. The inset shows the fitting results according to the thermal active model.

Figure 6:

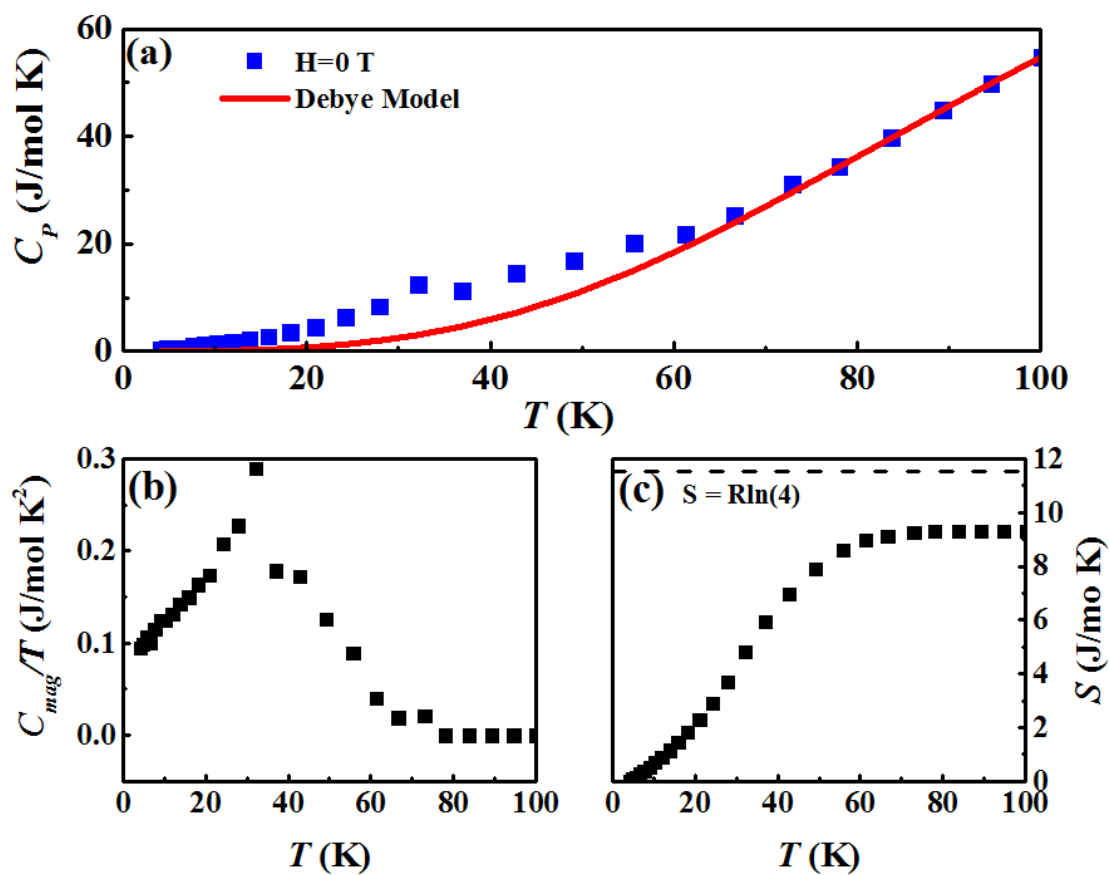


Fig. 6 (color online): (a) Heat capacity as a function of temperature under the applied magnetic field $H=0$ T. The solid line is the fitting line according to the Debye model. (b) C_{mag}/T vs. T . (c) The calculated magnetic entropy S_{mag} vs. T of CrPS₄ single crystal.

Figure 7:

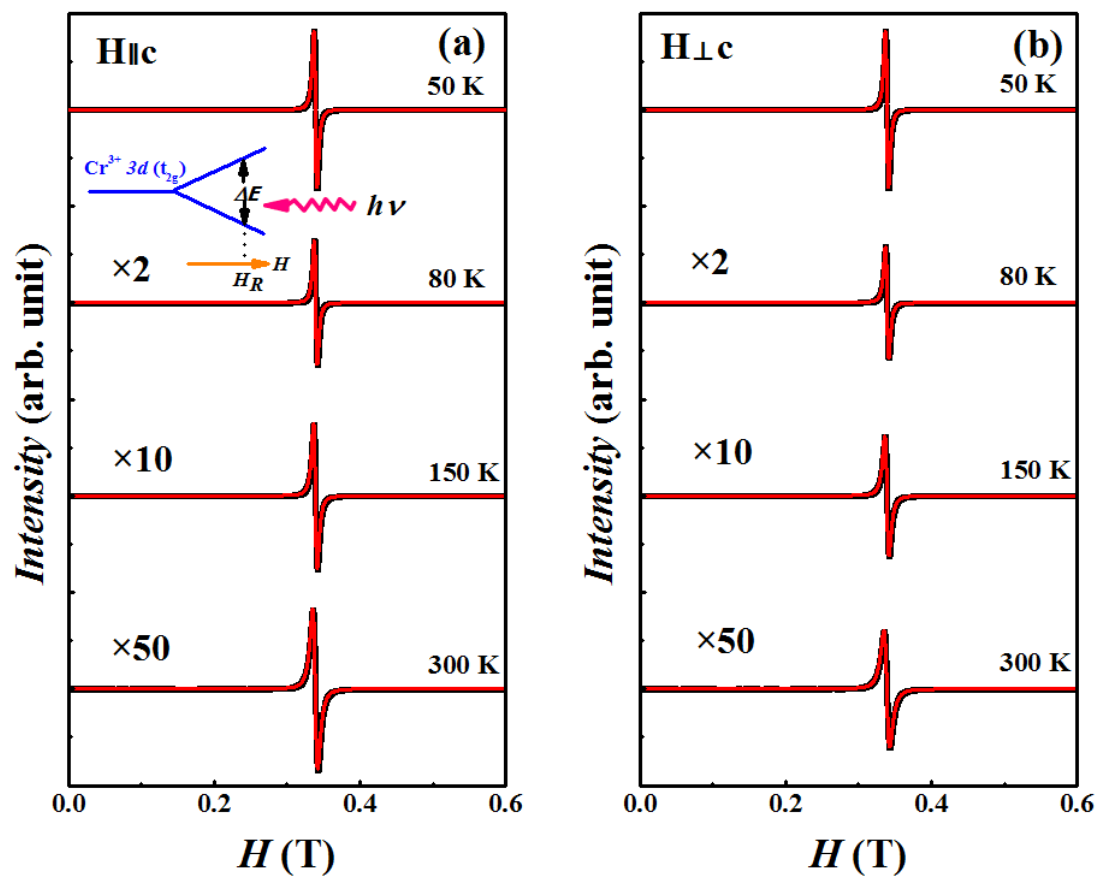


Fig. 7 (color online): The magnetic field dependence of ESR spectra along the different crystallographic axes. (a) for magnetic field parallel to the c axis and (b) for magnetic field perpendicular to the c axis. The red line is the fitting line according to a Lorentz shape.

Figure 8:

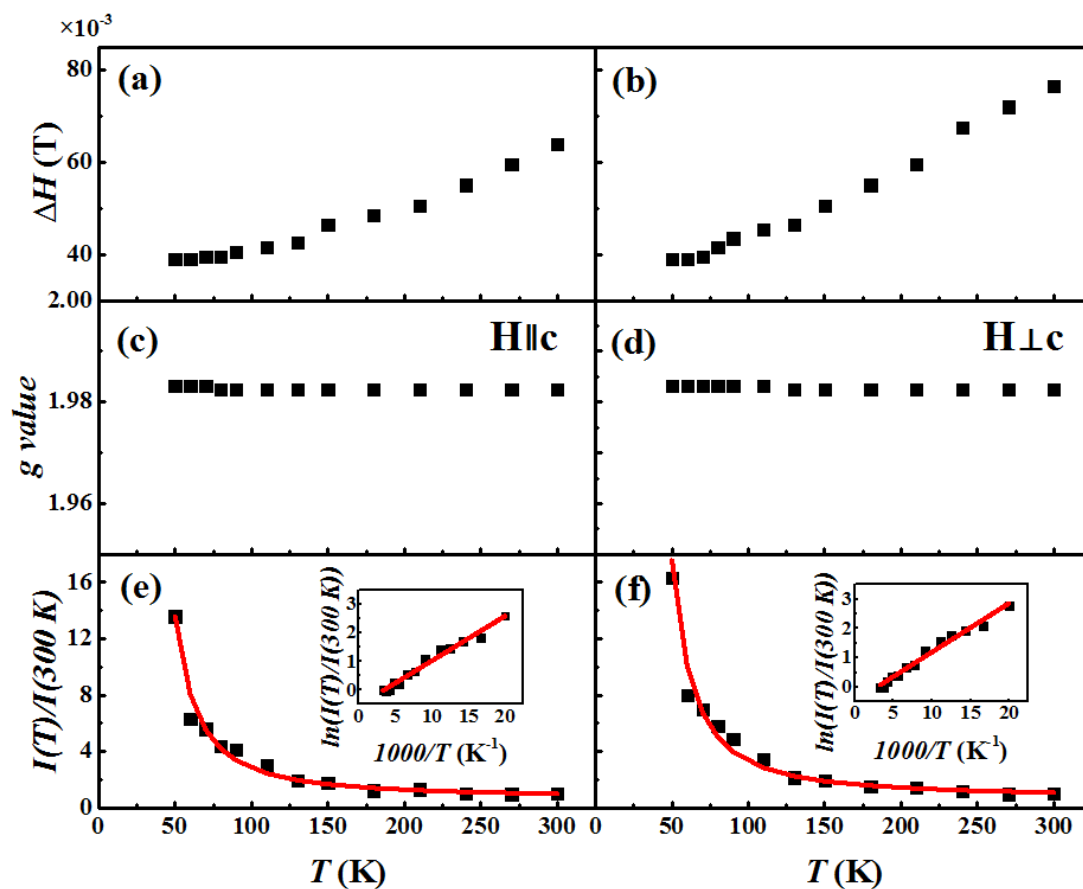


Fig. 8 (color online): (a) (b) The temperature dependence of HWHM (the half width at half maximum) ΔH along different crystallographic axes. (c) (d) The temperature dependence of the effective g values along different crystallographic axes. (e) (f) The normalized ESR intensity I by its value at 300 K vs. T of CrPS_4 single crystal. The red lines and the inset pictures show the fitting results according to the thermally activated model.

Figure 9:

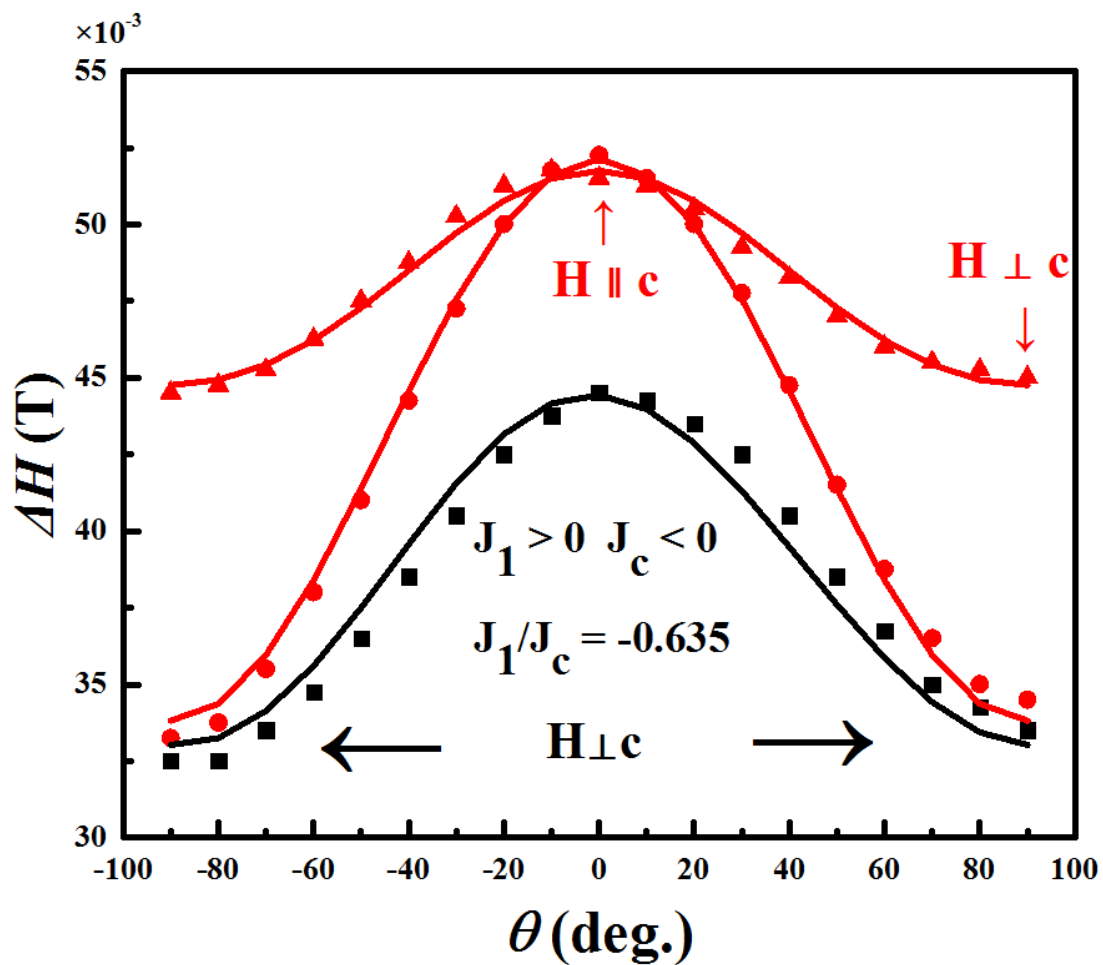


Fig. 9 (color online): Angular dependence of the HWHM (the half width at half maximum) ΔH and H_{res} for three crystallographic planes in different degrees. The solid lines show the fitting results of in-plane interaction and interlayer one.